

# Token Geometry

Kathan Shah

## Abstract

Language models learn continuous programs over discrete symbols, with the embedding table and LM-head acting as the read/write interface between them. We show that this interface has gradient geometry distinct from dense hidden weights which can be exploited to improve the Pareto frontier across supervised finetuning, RL, and pretraining, while only utilizing kilobytes of optimizer state. We introduce *Ember*, a lightweight optimizer for embedding and LM-head matrices that utilizes  $\mathcal{O}(V + D)$  VRAM, instead of Adam’s  $\mathcal{O}(2VD)$ , and forgoes the need to shard both token table optimizer states. We provide empirical evidence that Ember scales effectively across batch size and parameter count. We show that the optimization trajectory of tokens can be well described by a simple 1D ray, counter to the popular belief that neural net parameters navigate a heavily nonconvex landscape. We provide a principled view on the surprisingly narrow space of optimizers that suffice for Transformer training. Finally, we open-source our distributed Ember implementation that merges cleanly with existing ZeRO/FSDP setups to support further research ([github.com/katop1234/ember](https://github.com/katop1234/ember)).

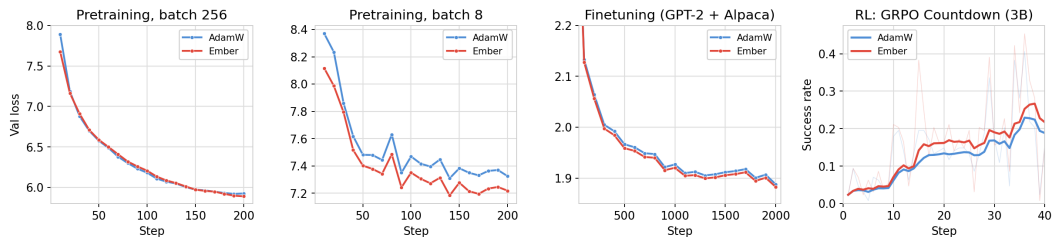


Figure 1: The Ember optimizer utilizes almost no optimizer state for the embedding table and LM-head, and universally matches or improves upon current SOTA. In the sparse gradients/low-batch regime (Fig 1B) Ember outperforms Adam by a wide margin, and in fine-tuning + RL (Fig 1C,1D), it achieves within-seed parity with Adam while doing better at most recorded checkpoints.

## 1 Introduction

Embedding and LM-head matrices, or “token interface” parameters, are currently optimized with Adam [1]. This is corroborated by a report from the current open source frontier, DeepSeek V4 [14], which only changed the optimizer for linear layers to Muon [15]. Of note, in literature, almost all proposed successors of Adam solely apply to linear layers and steer clear of the embedding table. Therefore improvements are pertinent as Adam requires significant distributed training engineering and doesn’t fully leverage the geometry of token interfaces. In this paper, we introduce *Ember*, a lightweight optimizer for such Transformer parameters that remedies these and achieves competitive results. We begin with some preliminaries on information geometry:

**The Fisher metric.** Under regularity assumptions, cross-entropy loss possesses a remarkable property: the second derivative for a given parameter is just the square of its first derivative,

$$-\mathbb{E}_{p_\theta} \left[ \frac{\partial^2}{\partial \theta_i^2} \log p_\theta(x) \right] = \mathbb{E}_{p_\theta} \left[ \left( \frac{\partial}{\partial \theta_i} \log p_\theta(x) \right)^2 \right].$$

also known as the Fisher Information metric [8, 9, 10], which near the optimum coincides with the Hessian of the cross-entropy loss. Although the standard optimization baseline is Newton’s method, which conditions each gradient with the inverse of its second derivative, standard backprop is not amenable to returning second derivatives cheaply. Fortunately, the Fisher, or second derivative, can be estimated cheaply using only the first derivative’s information as described above.

**Canonical Geometry of Cross-Entropy.** The Fisher metric is especially elegant because it is not merely useful as an approximation, but it is the exact second-order term of the Kullback–Leibler divergence:

$$D_{\text{KL}}(p_\theta \parallel p_{\theta+d\theta}) = \frac{1}{2} d\theta^\top F(\theta) d\theta + \mathcal{O}(\|d\theta\|^3).$$

By Chentsov’s theorem [6], for the KLD there exist no other canonical local geometry besides the Fisher. Therefore, optimization beyond SGD for cross-entropy loss must utilize this quantity; this is well-established as “natural gradient descent” [7, 2, 11, 12].

There are a few caveats, which are easily remedied. First, the Fisher, being a second order correction, assumes an exact quadratic loss landscape. Second, it is numerically unstable under batch gradient descent, as at any given training step we only observe empirical token frequency  $\hat{p}_i$ , not the exact  $p_i$ .

## 1.1 Related work

SGD [16] is the simplest form of gradient descent, and uses the backprop gradient scaled by the learning rate to update parameters. Adam [1] builds on it by dividing this by its RMS, and maintains a bias-corrected EMA of the 1st and 2nd moments which takes  $\mathcal{O}(2VD)$  memory per token table.

Lion [17] shows momentum on just the gradient sign is competitive. Muon [15] forces singular values of the gradient matrix for each dense linear layer to be unitary, and is used by frontier models. Adafactor [18] uses a similar form to Ember where it drops the first moment buffer of Adam entirely and factorizes the second moment, albeit with 4 additional configs. We note we independently converged on this setup which we elaborate on in App 6.5 and believe it lends further credence to our approach.

[19] claims that linear layers are fundamentally symmetric, so a good optimizer should leverage this rather than update its parameters as if they were a 1D concatenated vector. Modula [4, 13] was one of the first to present a grand unified theory of optimizers, mathematically grounded in norm duality. They derive that row-normalization is optimal for embeddings, corroborating the analysis of this paper.

### 1.1.1 Square-root Fisher metric

At a high level, we argue these optimizers share the same fundamental principle on top of SGD. Each paper uses varying terminology, but we find the most parsimonious explanation to be to “cast each gradient into a z-score” (mathematically, to condition with the square-root of the Fisher metric). Recall that the Fisher is just the squared gradient which equals its variance when the model is near an optimum. Therefore, dividing by its square root resembles a division by the standard deviation of the gradient estimator.

There is a sense that Adam captured this metric with its denominator, which, for a given parameter gradient  $g$ , conditions it on the order of  $(g^2)^{-1/2}$ . Curiously, one can show that the Muon optimizer parallels this, as it conditions the matrix gradient  $G$  with  $(G^T G)^{-1/2}$ . It is trivial to see this is precisely dividing by the square root of the matrix-variate analogue of the square of  $G$ . We claim this simple form comprises the set of competitive Transformer optimizers.

In standard optimization, it is a well known baseline to simply condition gradients by the inverse of curvature [21]. Strikingly, we argue that modern deep learning does only this with moderate

adjustments like applying the square root instead of the full curvature correction as an exact quadratic landscape cannot be assumed and we observe just a minibatch at each step.

Surprisingly, the literature in this field is splintered across various linear algebraic derivations or empirical findings, and does not lead with the Fisher despite it being a central mathematical object with easily manipulatable properties. Although these works seem to be conveying the same underlying concept, using a unified vocabulary around the Fisher (which is canonically justified as the second-order term of cross-entropy loss) can speed up research in this domain.

## 2 Methods

### 2.1 Derivation

We begin from the observation that Adam works extremely well across a wide range of deep learning tasks despite its relatively simple structure. We note Adam approximates the square root empirical Fisher metric per-parameter, as the square of gradients approximates the curvature, an assumption we will use for this paper as Adam has empirically worked well for all parameter classes. Of note, as the second derivative is technically averaged over all parameter pairs, we note the 2nd moment EMA term automatically adjusts for this throughout training as entangled parameters receive net lower gradients.

First, we find that completely removing the first moment’s EMA and replacing it with the instantaneous gradient favors performance (Figure 11), and saves  $V \times D$  optimizer state in both the input embedding table and the LM head.

We observe that row-wise gradient energy is an unbiased estimator for the probability of a token participating, which we denote as  $p_i$ . Intuitively, this is because backpropagation accumulates gradients every time a token is selected, so a token with higher frequency has gradient  $\ell_2$  norm proportional to that. Therefore, since the row-wise Fisher scales with  $p_i^2$  (App. 6.8), the curvature can be well approximated by  $V$  row-wise squared gradient EMAs rather than the standard  $V \times D$  buffer. As per standard optimizer literature, we apply bias correction, and take the square root of this curvature metric, which has the nice property that the net gradient is effectively a z-score in each row. Our first major discovery is that this switch saves significant memory ( $\approx D \times$ ) state and is at par with Adam (Fig. 2).

We continue from this, observing that this approach, although efficient, assigns each parameter in a token the same curvature by assuming feature-wise isotropy, which is not true in general. Therefore, to correct for this, we use an outer product with a cheap  $\mathcal{O}(D)$  column-wise factor (that is otherwise identical to the above following a transpose) to estimate the elementwise squared gradient (Fig. 12, App. 6.6) and observe that it surpasses or matches Adam in performance in benchmarks. Due to the vocab size being large, by the law of large numbers the column factor concentrates near unity so its contribution is marginal; thereby, in this paper we focus our analysis on the row-only version of Ember.

Including the column factor makes the denominator have an extra unit of  $g$ , so we derive that the mathematically optimal way to reduce variance (6.7) and match the units to the square-root Fisher is to divide the outer product by the geometric mean of the mean of the row and column buffer (Alg. 1).

Essentially, we drop the first moment from Adam and replace its second moment buffer with a cheap outer product of 1D row- and column-wise factors (Alg. 1) that reproduces the dense second moment pointwise (Fig. 12), and find it provides SOTA results when replacing Adam for the embedding table. The only hyperparameter is  $\beta_2 = 0.999$ , which we lift directly from the original Adam paper.

### 2.2 Optimizing sparsely activated parameters

Each token row participates in training at a different rate. Let  $p_i$  denote the frequency of token  $i$  activating under the training distribution,  $g_i$  its net gradient, and  $F_i = \mathbb{E}_z[\nabla_{\theta_i} \log p_{\theta}(z) \nabla_{\theta_i} \log p_{\theta}(z)^{\top}]$  the token Fisher. There exist a few mathematically valid views on scaling token gradients with  $p_i$ , and each choice corresponds to a different metric on the embedding table.

**Scale with  $p$ .** An elementary view on rescaling gradients is to let the update grow with participation so  $g_i \propto p_i$ , as intuitively the energy should scale with how confident we are about it. However, this

---

**Algorithm 1** *Ember*, our proposed optimizer for embedding and LM-head matrices. Ember maintains row and column second-moment estimates and forms a lightweight outer-product preconditioner. Default settings used throughout this work are  $\alpha = 10^{-3}$  and  $\beta_2 = 0.999$ .

---

**Require:**  $\alpha$ : learning rate  
**Require:**  $\beta_2 \in [0, 1)$ : momentum term for second-moment estimates  
**Require:**  $R_t(\theta)$ : reward at timestep  $t$   
**Require:**  $\theta_0 \in \mathbb{R}^{V \times D}$ : initial parameters of the embedding or LM-head matrix

- 1:  $r_0 \leftarrow \mathbf{0} \in \mathbb{R}^V$  ▷ Initialize row second-moment vector
- 2:  $c_0 \leftarrow \mathbf{0} \in \mathbb{R}^D$  ▷ Initialize column second-moment vector
- 3:  $t \leftarrow 0$  ▷ Initialize timestep
- 4: **while**  $\theta_t$  not converged **do**
- 5:    $t \leftarrow t + 1$
- 6:    $g_t \leftarrow \nabla_{\theta} R_t(\theta_{t-1})$  ▷ Compute gradient through backprop
- 7:    $r_t \leftarrow \beta_2 r_{t-1} + (1 - \beta_2) \text{mean}_j(g_t^2)$  ▷ Update row second moment
- 8:    $c_t \leftarrow \beta_2 c_{t-1} + (1 - \beta_2) \text{mean}_i(g_t^2)$  ▷ Update column second moment
- 9:    $\hat{r}_t \leftarrow r_t / (1 - \beta_2^t)$  ▷ Bias-correct row estimate
- 10:    $\hat{c}_t \leftarrow c_t / (1 - \beta_2^t)$  ▷ Bias-correct column estimate
- 11:    $s_t \leftarrow \sqrt{\hat{r}_t \hat{c}_t}$  ▷ Geometric-mean normalization
- 12:    $\tilde{v}_t \leftarrow \hat{r}_t \hat{c}_t^\top / s_t$  ▷ Form factored preconditioner
- 13:    $\theta_t \leftarrow \theta_{t-1} + \alpha g_t / (\sqrt{\tilde{v}_t} + 10^{-8})$  ▷ Ascend the reward  $R_t$
- 14: **end while**
- 15: **return**  $\theta_t$

---

Figure 2: Embedding-optimizer ablation at two batch sizes for GPT-2 small / FineWeb. Interestingly, the row-only version achieves near-parity with canonical Ember and Adam, indicating most of the curvature comes from the participation probability and at high batch sizes this can be estimated sufficiently.

Embedding optimizer	Val@200 (bs=8)	Val@200 (bs=256)	State
AdamW	7.325	5.897	$2VD$
Adafactor	7.311	6.137	$V+D$
<b>Ember (ours)</b>	<b>7.219</b>	<b>5.890</b>	$V+D$
Ember row-only	7.665	5.911	$V$
Ember col-only	10.899	7.958	$D$

can lead to dead learning as tokens are typically selected according to a power law and would bias towards learning n-gram statistics [3]. Mathematically, this corresponds to using the identity metric  $F_i = I$ , and is exactly what vanilla SGD does.

**Scale with  $1/p$ .** An alternative view is to step inversely with participation such that the conditioned update scales with  $1/p_i$ . This aids learning, as rare tokens get a larger update whenever they participate. We have  $F_i \propto p_i^2$ , so  $F_i^{-1} \propto 1/p_i^2$  and  $F_i^{-1} g_i \propto 1/p_i$  (App. 6.8). Mathematically, this corresponds to the full Fisher correction and one-shots the optimum in the full-batch, quadratic regime.

**Scale isotropically.** A more balanced view is that parameter updates should be isotropic, that is, independent of  $p$ . For example, if Token A is observed 10% of the time, and Token B 0.1% of the time, it makes sense to scale Token B’s gradient by  $100\times$  to match that of Token A. We do not discard the frequency information, as Token A still enjoys having  $100\times$  less variance in its update. Ember explicitly applies the same  $1/p$  correction through its row factor, which yields the nice property that the net update has no dependence on  $p$ , while its variance decreases as  $\text{Var}(\hat{g}_i) \propto 1/p_i$ .

### 2.2.1 Interpreting the metric

The last case above applies the square root Fisher metric, which has the interesting effect that the conditioned gradient is *unitless*, and at any given step, the model’s prior on the optima is a Gaussian ball centered at the current parameter vector with radius of the learning rate. In plain terms, we

Table 1: Supervised fine-tuning validation loss at step 250 across GPT-2 and Pythia model scales, with per-model embedding-optimizer state. Ember matches or improves over AdamW in all but the smallest Pythia setting while reducing token-interface optimizer state from  $\mathcal{O}(2VD)$  to  $\mathcal{O}(V+D)$ . State is fp32 optimizer buffers.

Model	Params (M)	AdamW	Ember	$\Delta$	AdamW state	Ember state
distilgpt2	82	2.3640	<b>2.3578</b>	-0.0062	309 MB	199 KB
gpt2	124	2.0456	<b>2.0381</b>	-0.0075	309 MB	199 KB
gpt2-medium	350	1.7467	<b>1.7430</b>	-0.0037	412 MB	200 KB
gpt2-large	774	1.5900	<b>1.5888</b>	-0.0012	515 MB	201 KB
pythia-160m	160	<b>2.4782</b>	2.5136	+0.0354	618 MB	399 KB
pythia-1.4b	1400	1.4309	<b>1.4306</b>	-0.0003	1.65 GB	409 KB
pythia-2.8b	2800	1.3527	<b>1.3519</b>	-0.0008	2.06 GB	413 KB

z-score the gradient over some basis (in Adam/Lion it’s per-parameter, Ember per-neuron, Muon per-singular value, etc.). In this sense, the learning rate is not the ideal term for this hyperparameter, but something along the lines of “trust region” is more apt. The Adam paper explicitly denotes this [1, Section 2.1].

We find that all SOTA optimizers are essentially just utilizing this metric along some basis transform and supplementing it for numerical stability and stochasticity. For example, signSGD [20] is equal to Adam with no EMA terms, and is exactly what a z-score cast into ‘1-bit precision’ resembles. Intuitively, this is the most conservative version of the square-root Fisher conditioned gradient, where the geometry tells us to trust nothing beyond 1 bit of its information. We believe the simple framing of this metric can be used to narrow the search space for training arbitrary Transformer parameters.

Interestingly, Muon [15], which normalizes the singular values of linear layer gradients, also is exactly applying the inverse square-root Fisher metric (App. 6.9). Embedding tables behave like linear layers, with the key distinction that their inputs are strictly one-hot encoded vectors and not continuous over the reals. There is no real sense of entanglement between rows, as the input space is either 0 or 1, so the singular vectors targeted by Muon no longer correspond to meaningful directions in the input space. The most natural curvature correction is therefore row- (token-)wise, where the analogue of singular vectors becomes the token gradient vectors themselves and singular values reduce to their  $\ell_2$  norms. The gradient matrix for the LM-head is just a smoothed version of that of the embedding table, and therefore, admits the same analysis (App. 6.10). Since these weights used to be tied in early LLMs, this is also empirically validated.

### 3 Analysis

#### 3.1 Scaling laws

**Model size** Ember matches AdamW as model size increases while removing the  $\mathcal{O}(2VD)$  optimizer state on the 2 token tables (Fig. 3). On GPT-2, Ember improves validation loss at every scale. On Pythia, the only visible residual is at 160M, and this gap vanishes by 1.4B (Table 1). These results suggest that, at larger scale, AdamW’s embedding-table second moment is well approximated by Ember’s rank-1 factorization.

We visually depict the optimizer state benefit in Fig. 4. Notably, on Pythia-2.8B, AdamW’s token-interface state reaches 2 GB, whereas Ember stays at 400 KB. This is a  $4,900\times$  reduction for the same val loss.

**Batch size** We find that Ember obeys the same near-linear law in log-batch across nine doublings and achieves validation loss within seed noise of AdamW. As a bonus, AdamW exhibits severe early-training loss spikes at batch sizes  $\leq 2$ , while Ember remains stable at every rung (Figure 8).

#### 3.2 Optimization Landscape

We analyzed the trajectory individual embedding tokens take from initialization to convergence by taking the SVD of the token vector concatenated over the  $T$  training steps into an  $\mathbb{R}^{D\times T}$  matrix, and

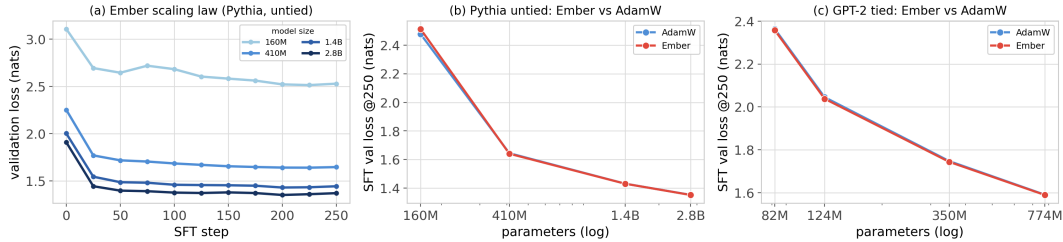


Figure 3: **Model-scaling results for Ember on token tables.** Ember scales cleanly with model size, and matches or surpasses Adam regardless of scale. Training setup in Appendix 6.2.

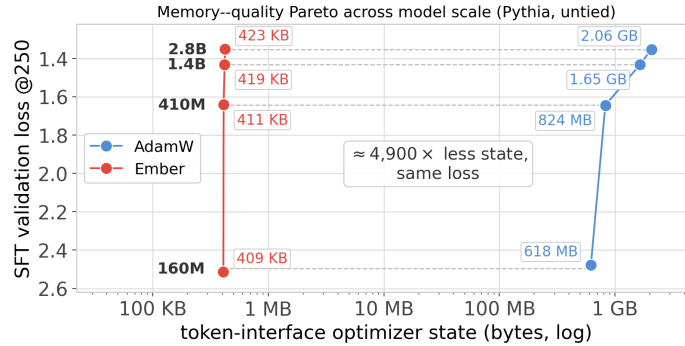


Figure 4: **The memory-quality gap widens with model scale.** The two optimizers reach the same loss at every scale, yet AdamW’s state grows as  $\mathcal{O}(2VD)$  — crossing 1 GB by 1.4B and reaching  $\sim 2$  GB at 2.8B — while Ember’s  $\mathcal{O}(V+D)$  state stays near 400 KB.

unexpectedly observed that it decomposes separably into a monomial basis (Fig. 5, 7). We look at which powers are above the noise floor and find that PC1 explains nearly 90% of the variance in the trajectory, which is unexpectedly high as it implies a simple 1-D ray explains how an LLM embedding table fits to FineWeb. As per the conventionally proclaimed nonconvexity of loss landscapes, one would have expected to see sudden jumps, oscillations, or dependence on many principal components. However, notably, we indicate this was not the case, as it resembles an extremely smooth path.

We claim that surprisingly, as higher order monomial terms fall below the observed noise floor, the optimization trajectory is not chaotic or weaving through multiple local optima; under the Ember update rule, it is mostly marching along a straight line from initialization to convergence.

## 4 Results

**Reinforcement learning.** We compare Ember against AdamW on the token tables when post-training Qwen2.5-3B-Instruct with GRPO [5] on the Countdown reasoning task, sweeping the rollout batch size from 64 to 256 (Fig. 6). Across all batch sizes, the two optimizers are indistinguishable within seed noise, while Ember uses only 600 KB of optimizer state compared to AdamW’s 2.5 GB (a 4040 $\times$  reduction).

**FineWeb pretraining.** On GPT-2-small with Muon on linear layers, Ember matches AdamW validation loss and beats Adafactor by 0.25 nat at identical  $V+D$  memory (Fig. 1, Fig. 2). In the low-batch regime, Ember particularly outperforms due to the stability of the rank 1 gradient decomposition, which we believe makes Ember well suited to when gradients are sparse/noisy.

**Autoregressive image generation.** Ember is competitive in computer vision tasks: on LlamaGen image-AR, using 1500 $\times$  less optimizer state, Ember is virtually indistinguishable from Adam (Fig. 9). Setup in Appendix 6.2.

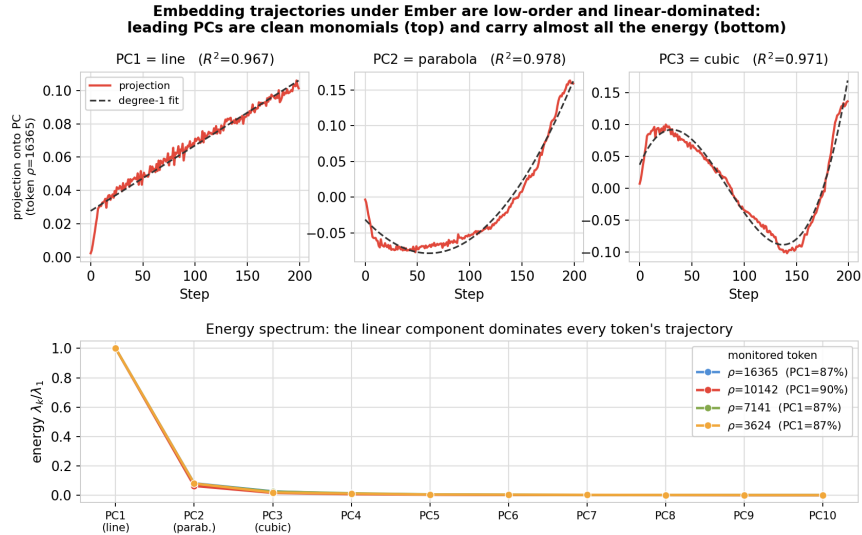


Figure 5: **Token optimization trajectories under Ember admit a clean polynomial structure.** We show how strongly the monomials fit the first 3 principal component projections and show indeed the Taylor series decomposition holds surprisingly well. Moreover, in the energy spectrum, the linear component significantly dominates across tokens, indicating the overall trajectory can be approximated surprisingly simply by a 1D ray. More examples can be found in Figure 7.

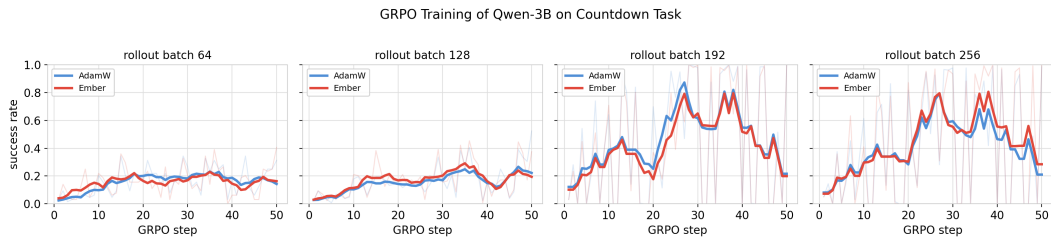


Figure 6: **Ember is competitive in reinforcement learning while removing  $\mathcal{O}(2VD)$  optimizer state.** AdamW and Ember achieve parity across rollout regardless of rollout batch size 64, 128, 192, and 256.

## 5 Discussion

We open-source a distributed version of Ember compatible with ZeRO [22]. Because Ember’s optimizer state is  $\mathcal{O}(V + D)$ , the embedding table optimizer state no longer requires sharding, simplifying distributed training setups. The implementation is available at [github.com/katop1234/ember](https://github.com/katop1234/ember).

### 5.1 Practical implications

**Faster iteration.** The overwhelming majority of experimentation is done on models  $\leq 7B$  parameters where Adam’s embedding state is a genuine binding constraint. For example, for Qwen2.5-7B, Adam stores roughly 8.72 GB VRAM for the token interface alone. Ember reduces this to about 1.2 MB. We believe the implications of this are significant as it allows much faster iteration on a single device without needing distributed training setups.

**Cleaner engineering.** The optimizer state for LayerNorm and the embedding tables are all 1-D and can fit on a single GPU across even the largest models. Only linear layers/MoE require sharding, which can be done more simply as they scale cleanly with model depth and number of experts per layer.

**Multiple embedding tables.** The savings scale with  $V \cdot D$ , substantial for large-vocabulary or multimodal models where modalities each carry their own embedding table. Google’s recent Gemma

3n models include Per-Layer Embedding [27], where each layer gets its own embedding table; presumably, these would have significant optimizer state and Ember would be even more useful there.

## 5.2 Conclusion

Our experiments demonstrate that Ember can effectively replace Adam as the de-facto Embedding table and LM-head optimizer while using virtually no optimizer state memory. We claim that even if Ember even slightly lagged Adam in performance, it should still be preferable for embedding tables due to its significant memory savings, as its optimizer state no longer has to be sharded and can fully fit in a single GPU. We believe the theoretical implications of understanding token table geometry can help us understand how LLMs learn. We show that the optimization trajectory is surprisingly well-behaved and decomposes into a clean monomial basis.

## References

- [1] Diederik P. Kingma and Jimmy Ba. Adam: A method for stochastic optimization. In *International Conference on Learning Representations (ICLR)*, 2015.
- [2] Sham M. Kakade. A natural policy gradient. In *Advances in Neural Information Processing Systems 14*, pages 1531–1538. MIT Press, 2001.
- [3] Frederik Kunstner, Robin Yadav, Alan Milligan, Mark Schmidt, and Alberto Bietti. Heavy-tailed class imbalance and why Adam outperforms gradient descent on language models. In *Advances in Neural Information Processing Systems*, 2024.
- [4] Jeremy Bernstein and Laker Newhouse. Modular duality in deep learning. In *arXiv preprint arXiv:2410.21265*, 2024.
- [5] Zhihong Shao, Peiyi Wang, Qihao Zhu, Runxin Xu, Junxiao Song, Xiao Bi, Haowei Zhang, Mingchuan Zhang, Y. K. Li, Y. Wu, and Daya Guo. DeepSeekMath: Pushing the limits of mathematical reasoning in open language models. *arXiv preprint arXiv:2402.03300*, 2024.
- [6] N. N. Chentsov. *Statistical Decision Rules and Optimal Inference*. Translations of Mathematical Monographs, Vol. 53. American Mathematical Society, Providence, RI, 1982.
- [7] Shun-ichi Amari. Natural gradient works efficiently in learning. *Neural Computation*, 10(2):251–276, 1998.
- [8] Shun-ichi Amari. *Information Geometry and Its Applications*. Applied Mathematical Sciences, Vol. 194. Springer Japan, Tokyo, 2016.
- [9] Alexander Ly, Maarten Marsman, Josine Verhagen, Raoul P. P. P. Grasman, and Eric-Jan Wagenmakers. A tutorial on Fisher information. *Journal of Mathematical Psychology*, 80:40–55, 2017.
- [10] Frank Nielsen. An elementary introduction to information geometry. *Entropy*, 22(10):1100, 2020.
- [11] Razvan Pascanu and Yoshua Bengio. Revisiting natural gradient for deep networks. In *International Conference on Learning Representations (ICLR)*, 2014.
- [12] Guillaume Desjardins, Karen Simonyan, Razvan Pascanu, and Koray Kavukcuoglu. Natural neural networks. In *Advances in Neural Information Processing Systems*, 2015.
- [13] Jeremy Bernstein. Modular manifolds. *Thinking Machines Lab: Connectionism*, 2025. <https://thinkingmachines.ai/blog/modular-manifolds/>, doi:10.64434/tml.20250926.
- [14] DeepSeek-AI. DeepSeek-V4: Towards highly efficient million-token context intelligence. *Technical Report*, 2026.
- [15] Keller Jordan. Muon: An optimizer for LLMs. *Keller Jordan’s Blog*, 2024. URL: <https://kellerjordan.github.io/posts/muon/>.
- [16] David E. Rumelhart, Geoffrey E. Hinton, and Ronald J. Williams. Learning representations by back-propagating errors. *Nature*, 323(6088):533–536, 1986.
- [17] Xiangning Chen, Chen Liang, Da Huang, Esteban Real, Kaiyuan Wang, Yao Liu, Hieu Pham, Xuanyi Dong, Thang Luong, Cho-Jui Hsieh, Yoram Singer, and Quoc V. Le. Symbolic discovery of optimization algorithms. *arXiv preprint arXiv:2302.06675*, 2023.
- [18] Noam Shazeer and Mitchell Stern. Adafactor: Adaptive learning rates with sublinear memory cost. In *International Conference on Machine Learning (ICML)*, 2018.
- [19] Tim Tsz-Kit Lau and Weijie Su. Symmetry-compatible principle for optimizer design: Embeddings, LM heads, SwiGLU MLPs, and MoE routers. *arXiv preprint arXiv:2605.18106*, 2026.

- [20] Jeremy Bernstein, Yu-Xiang Wang, Kamyar Azizzadenesheli, and Anima Anandkumar. signSGD: Compressed optimisation for non-convex problems. In *International Conference on Machine Learning (ICML)*, 2018.
- [21] Jorge Nocedal and Stephen J. Wright. Numerical optimization. Springer, 2nd edition, 2006.
- [22] Samyam Rajbhandari, Jeff Rasley, Olatunji Ruwase, and Yuxiong He. ZeRO: Memory optimizations toward training trillion parameter models. In *International Conference for High Performance Computing, Networking, Storage and Analysis (SC20)*, 2020.
- [23] M. S. Bartlett. Approximate confidence intervals. In *Biometrika*, 1953.
- [24] Francis Ysidro Edgeworth. The law of error. In *Transactions of the Cambridge Philosophical Society*, 20:33–66, 1905.
- [25] Shun-ichi Amari. *Differential-Geometrical Methods in Statistics*. Lecture Notes in Statistics, Volume 28. Springer, 1985.
- [26] Nikolai N. Chentsov. *Statistical Decision Rules and Optimal Inference*. American Mathematical Society, 1982.
- [27] Google AI. *Gemma 3n model overview*. 2025. <https://ai.google.dev/gemma/docs/gemma-3n>. Accessed: 2026-06-17.

## 6 Appendix

### 6.1 Further work

**Parameter class-awareness.** In general, a principled method of coming up with optimizers for different transformer parameter classes can likely save memory state and improve performance. Comfortingly, the search space of valid optimizers will fall with a narrow band of conditioning with the square root Fisher, which seems to be mathematically principled and empirically has worked well so far.

**The full Fisher.** We note that the true Fisher is actually a full  $N \times N$  matrix, where  $N$  is the number of parameters in a model. This work, along with other leading optimizers to date, are effectively utilizing a sparse diagonal or block-diagonal version of it where  $< 1\%$  of it is populated, so further work could investigate how to expand beyond this.

**Beyond the Fisher.** There also exist correction terms for higher order terms in the Kullback-Liebler divergence beyond the Fisher. These are surprisingly extremely GPU-friendly through the Bartlett identities [23, 24, 25, 26] which maps the  $n$ -th derivative of the score function to its  $n$ -th statistical moment (recall the Fisher is just the variance of the score, so the generalized third derivative would just be its skew, etc.).

In general, learning algorithms that tailor to the full Taylor-series expansion of cross-entropy can be foundational to the next phase of deep learning. In RL where gradients are notoriously sparse, such an optimizer can learn how to fit a single top-quality sample, rather than rely on hundreds of medium-to-high quality ones (if they even exist). This direction can even introduce a new scaling law along the size of the optimizer state.

### 6.2 Experimental details

**Scaling parameter count** All model-scaling runs finetune on Alpaca SFT for 250 steps with effective batch size 128, learning rate  $2 \times 10^{-5}$  with cosine decay, and bf16 precision. The transformer body uses AdamW throughout; only the *token-embedding / LM-head* optimizer is varied.

**Scaling batch size** We train GPT-2-small ( $V = 50257$ , block 144) on FineWeb with both token tables untied, sweeping the batch size across nine doublings from 1 to 512 for 300 steps (seed 1) and reporting validation loss at step 200.

**Autoregressive image generation.** LlamaGen is a vanilla decoder-only transformer that generates images autoregressively. Instead of predicting over discrete language tokens, it trains its own learnable embedding table to look up within a frozen VQGAN codebook. We ablated Adam versus our optimizer using the same learning rate of  $1 \times 10^{-4}$  on LlamaGen image-AR.

### 6.3 Supplementary figures

A note on terminology: each principal component  $k$  of the trajectory is dominated by its leading power  $t^k$  (PC1 linear, PC2 quadratic, PC3 cubic, ...), and we use *monomial basis* to denote this degree-ordered structure.

### 6.4 Ablations

**Bias correction.** Bias correction is crucial to Ember’s performance, and allows it to plug-and-play with existing Adam setups (Fig. 10).

**Nesterov look-ahead ablation.** We ran a  $3 \times 3$  grid over  $\beta_2 \in \{0.999, 0.95, 0.9\}$  and learning rate  $\text{lr} \in \{5 \times 10^{-4}, 10^{-3}, 2 \times 10^{-3}\}$ , and consistently found that injecting the current  $g^2$  estimate into the denominator hurts performance across all learning rates. Intuitively, the second moment acts as a smooth scale/curvature estimate and should not react to instantaneous gradients. Canonical  $\beta_2 = 0.999$  was already optimal.

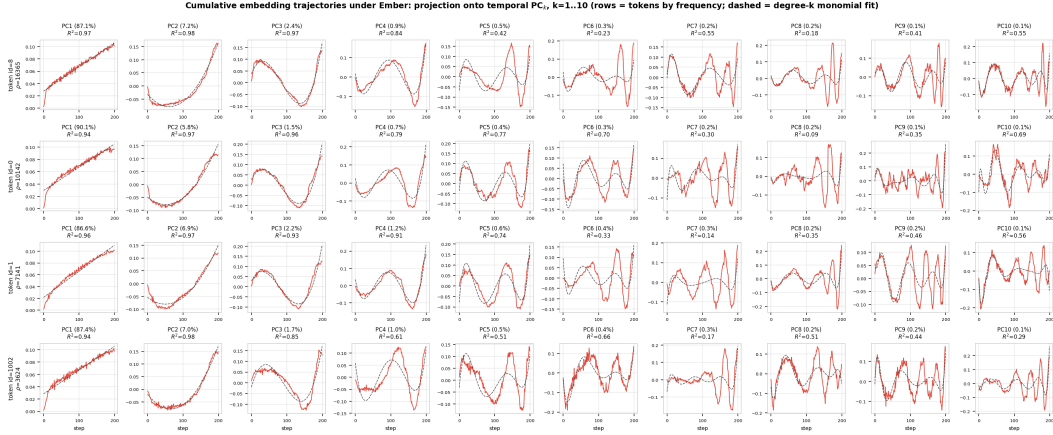


Figure 7: For each of four monitored tokens, we stack it over the time-axis to get  $\theta(t) \in \mathbb{R}^{D \times T}$  and take its SVD. Each cell plots the projection onto the  $k$ -th principal component, for  $k = 1, \dots, 10$ . Nontrivially, we find that the trajectory projected onto the principal components forms a clean monomial basis: PC1 is a straight line, PC2 a parabola, PC3 a cubic, PC4 a quartic, etc. Clean polynomial projections on PCs would not appear when the trajectory is noise-dominated or chaotic. Moreover, because the polynomial decomposition works well here, we can analyze how strong the first few powers fit, and show that surprisingly PC1, a linear ray, explains roughly 90% of the trajectory.

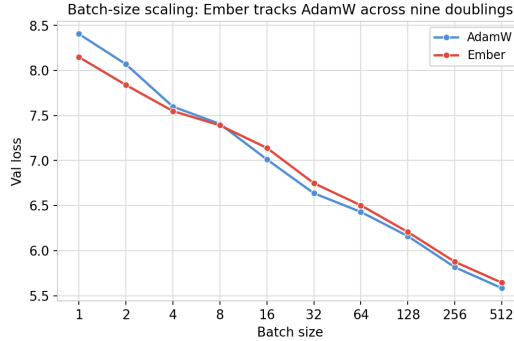


Figure 8: Batch-size scaling. Ember follows AdamW’s log-batch trend and remains within seed noise across nine batch-size doublings.

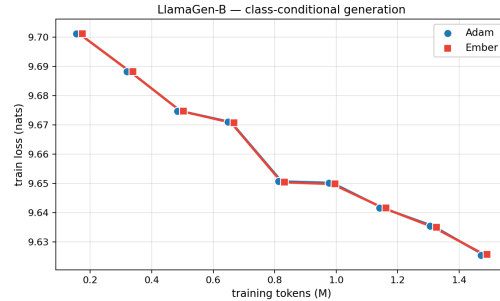


Figure 9: Autoregressive image generation results. Ember matches Adam while using substantially less optimizer state.

## 6.5 Comparison to Adafactor

Incidentally, we independently converged on a similar optimizer structure to Adafactor, with both methods relying primarily on factored second moments while removing first-moment momentum. Adafactor derives this from a KL-optimal linear algebraic view of Adam’s second moment term, whereas we arrive at nearly the same form from Fisher geometry. Since the Fisher metric is itself the canonical second-order approximation to KL divergence,

$$\text{KL}(p_\theta \parallel p_{\theta+\delta\theta}) \approx \frac{1}{2} \delta\theta^\top F \delta\theta,$$

both methods can be viewed as solving the same variational problem from different perspectives. We find the fact that two independent theories converged to the same optimizer family to be even stronger evidence for our method. In fact, Adafactor was developed by one of the creators of the Transformer, Noam Shazeer, indicating this form factor may be very foundational.

**Reduced complexity.** Adafactor uses four unique tricks in their paper to make it converge, which is less desirable to the modern deep learning practitioner due to the overhead of managing the entire stack. They are: (1) `decay_rate`, starts at  $\beta_2 = 0$  and grows — replaces bias correction

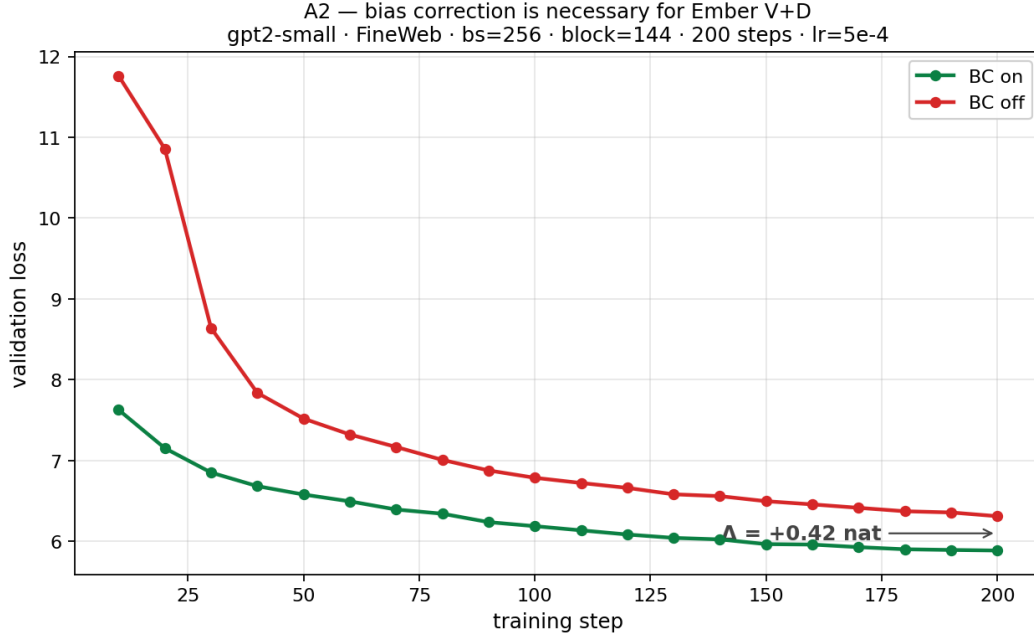


Figure 10: **Ablating bias correction in Ember.** Including the bias correction is crucial to performance and makes training much stabler while helping the optimizer reach lower val loss faster.

(2) `relative_step = min(10-2, 1/√t)`, which replaces the learning rate (3) `scale_parameter`, which makes step size proportional to parameter scale (4) `clip_threshold = 1.0`, post-hoc RMS clipping. We observe that including the bias correction term cleanly avoids needing these tricks (Fig. 10) and makes our optimizer easily plug-and-play with an existing Adam setup.

**Token-focused optimization.** The original Adafactor proposes applying it to linear layers also, and we’ve observed such methods perform subpar there, and Muon-esque optimizers are extremely tuned for this parameter class anyway. We believe the idea of outer product second moment applies best to embedding matrices, which haven’t seen any optimization advancements in 5+ years as of writing this paper. We deliberately do not recommend using Ember for dense linear layers.

## 6.6 Decomposing the Squared Gradient

We justify why the dense  $V \cdot D$  second moment  $\mathbb{E}[g_{ij}^2]$  is well approximated by a rank-1 outer product, which is what licenses Ember’s  $\mathcal{O}(V+D)$  state.

For an embedding/LM-head matrix  $\theta \in \mathbb{R}^{V \times D}$ , the per-example gradient is an *outer product*. Writing the upstream (output-side) signal as  $\delta \in \mathbb{R}^V$  and the input-side vector as  $x \in \mathbb{R}^D$ ,

$$g_{ij} = \delta_i x_j \quad \implies \quad g_{ij}^2 = \delta_i^2 x_j^2.$$

The two factors are concretely:

- **Input embedding.**  $x$  is a one-hot token selector, so  $\delta$  is the gradient of the selected row and  $\mathbb{E}[g_{ij}^2] = p_i \mathbb{E}[u_j^2]$ , where  $p_i$  is the participation frequency of token  $i$  and  $u$  the back-propagated embedding gradient. Thus the row factor is the participation curvature  $R_i \propto p_i$  (cf. App. 6.8).
- **LM head.**  $\delta_i = (p_i - \mathbf{1}[y = i])$  is the softmax error and  $x_j = h_j$  is the hidden state, giving  $\mathbb{E}[g_{ij}^2] = \mathbb{E}[\delta_i^2] \mathbb{E}[h_j^2]$ , i.e. the per-token error energy times the per-feature hidden energy.

WHY Ember works on both vocab tables (input embedding + output head)

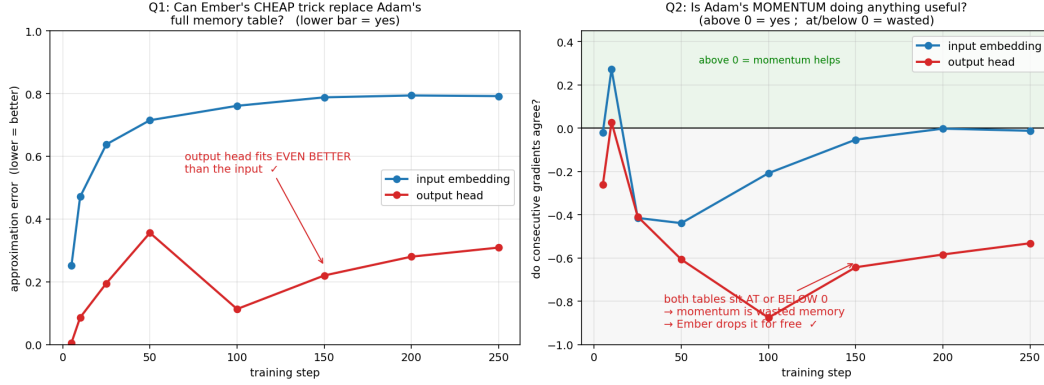


Figure 11: **Why removing Adam’s first-moment state is safe on token tables.** We instrument gradients of the untied input embedding  $E_{\text{in}} \in \mathbb{R}^{V \times d}$  and output head  $W_{\text{out}} \in \mathbb{R}^{V \times d}$  during GPT-2 small training on FineWeb. Left: Ember’s row-column factored second moment approximates the dense squared-gradient structure, where the y-axis is relative error. Right: temporal gradient autocorrelation is near zero or negative, showing that first-moment momentum carries little useful signal on token tables. Together, these explain why Ember can drop Adam’s dense first moment while preserving or improving performance.

In both cases, taking expectations and using that the output-side energy  $\delta_i^2$  and the input-side energy  $x_j^2$  are (to first order) uncorrelated across the data,

$$\mathbb{E}[g_{ij}^2] = \underbrace{\mathbb{E}[\delta_i^2]}_{R_i} \underbrace{\mathbb{E}[x_j^2]}_{C_j}$$

which is exactly rank-1. The row buffer  $\hat{r}_i$  estimates  $R_i$  (output/token curvature) and the column buffer  $\hat{c}_j$  estimates  $C_j$  (input/feature energy), so their outer product reconstructs the dense diagonal Fisher up to the residual cross-correlation  $\text{Cov}(\delta_i^2, x_j^2)$ . This residual is what Fig. 12 measures empirically and finds negligible (pointwise correlation 0.974 across ten orders of magnitude), confirming the dense  $V \cdot D$  second moment is captured by a  $V+D$  factorization.

Fig. 12 tests the outer product estimates the dense second moment matrix effectively. We collected the empirical squared gradient  $\hat{g}_{ij}^2 = \sum_t g_{ij,t}^2 / T$  for all 38M embedding parameters during a 500-step gpt2-small run on FineWeb, and compared it pointwise to Ember’s factored estimate. Ember’s  $V+D$  factored proxy closely tracks Adam’s full  $V \cdot D$  diagonal, capturing most of its structure. At the aggregate level, the effective second-moment scale  $f_{\text{Ember}}$  matches Adam’s  $f_{\text{Adam}}$  to within 5% at every logged step after initialization.

### 6.7 Outer Product Unit Alignment

Having established  $\mathbb{E}[g_{ij}^2] \approx R_i C_j$ , we derive the correct normalization of the outer product. Each buffer is a mean of squared gradients, so  $\hat{r}_i$  and  $\hat{c}_j$  carry units of  $[g]^2$ . The raw outer product therefore carries units  $[g]^4$ :

$$\hat{r}_i \hat{c}_j \sim [g]^2 \cdot [g]^2 = [g]^4.$$

For the update  $g_{ij} / (\sqrt{\tilde{v}_{ij}} + \epsilon)$  to be dimensionless — a z-score, matching the square-root Fisher metric — we require  $\sqrt{\tilde{v}_{ij}} \sim [g]$ , i.e.  $\tilde{v}_{ij} \sim [g]^2$ . The outer product thus carries one extra factor of  $[g]^2$  that must be removed by dividing by a scalar of units  $[g]^2$ .

The unique scalar built symmetrically from the two marginals with the correct units is their geometric mean,

$$s = \sqrt{\hat{r} \hat{c}}, \quad \bar{r} = \text{mean}_i \hat{r}_i, \quad \bar{c} = \text{mean}_j \hat{c}_j,$$

giving  $\tilde{v}_{ij} = \hat{r}_i \hat{c}_j / s \sim [g]^2$  as required. Because the mean of the row-means equals the grand mean of  $g^2$ , which also equals the mean of the column-means, one has  $\bar{r} = \bar{c}$ ; the geometric mean makes

Figure 2 — outer-product factorization (Ember V+D vs dense V:D)  
 OLS slope  $\beta=0.929$  intercept  $\alpha=+0.02$  Pearson  $r=0.897$   $R^2=0.805$   $n=37.2M$  entries

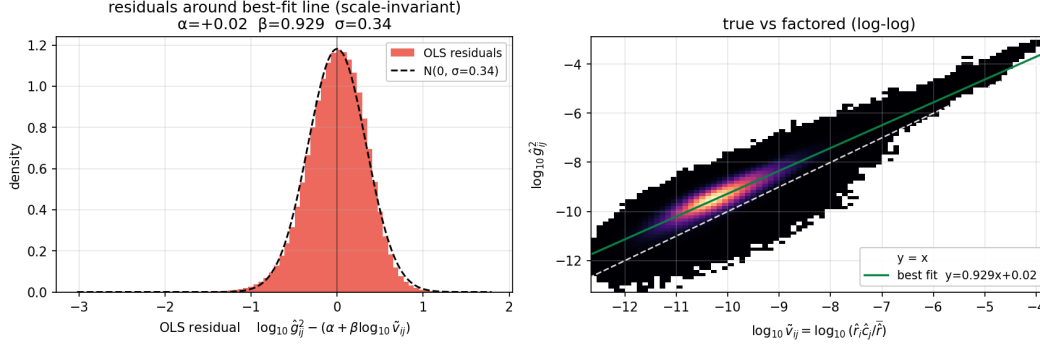


Figure 12: Ember’s  $V+D$  factored second moment closely tracks the dense Adam second moment. Right: each point is one embedding parameter  $(i, j)$ ; the factored estimate  $\hat{r}_i \hat{c}_j / \bar{r}$  tracks the dense  $\hat{g}_{ij}^2$  across many orders of magnitude. Left: log-space residuals concentrate near zero with no heavy tail, showing that most dense curvature structure is captured by the row/column outer product. Pointwise, the match holds across ten orders of magnitude with a correlation of 0.974 with OLS slope 0.93 (which is consistent with an unbiased estimator with sub-unity slope due to implicit regularization from noise). The log-space residuals concentrate near zero with no heavy tail.

the row/column symmetry explicit and remains the stable choice under finite-sample fluctuations where the two marginals differ.

**Exactness.** If the second moment is genuinely rank-1,  $\mathbb{E}[g_{ij}^2] = a_i b_j$ , then  $\hat{r}_i = a_i \bar{b}$ ,  $\hat{c}_j = \bar{a} b_j$ , and  $s = \bar{a} \bar{b}$ , so

$$\tilde{v}_{ij} = \frac{\hat{r}_i \hat{c}_j}{s} = \frac{(a_i \bar{b})(\bar{a} b_j)}{\bar{a} \bar{b}} = a_i b_j,$$

i.e. the geometric-mean normalization recovers the true element exactly and without bias.

**Variance optimality.** The geometric mean in linear space is the arithmetic mean in log space. Modeling the per-step estimate multiplicatively as  $g_{ij}^2 = a_i b_j \eta_{ij}$  with log-noise  $\log \eta_{ij}$ , the recovered statistic

$$\log \tilde{v}_{ij} = \log \hat{r}_i + \log \hat{c}_j - \log s$$

is exactly the two-way (row + column) additive decomposition of  $\log g_{ij}^2$ , whose marginal-mean estimator is the maximum-likelihood / minimum-variance estimator of the row and column effects under log-Gaussian noise. Intuitively,  $\hat{r}_i$  pools  $D$  entries and  $\hat{c}_j$  pools  $V$  entries, so the factored estimate has relative variance  $\mathcal{O}(1/V + 1/D)$  against  $\mathcal{O}(1)$  for the raw single-sample  $g_{ij}^2$ . Dividing by the geometric mean is therefore the unique normalization that is simultaneously unit-correct, unbiased on rank-1 structure, and variance-optimal.

## 6.8 The Fisher is proportional to inverse frequency squared

**Frequency scaling of the row-wise Fisher.** Let token  $i$  have data frequency  $p_i$ , so in a batch of size  $B$  its number of occurrences is the random count  $K_i \sim \text{Binomial}(B, p_i)$ , with

$$\mathbb{E}[K_i] = Bp_i, \quad \mathbb{E}[K_i^2] = Bp_i(1 - p_i) + B^2 p_i^2.$$

Let  $h_{i,k}$  denote the per-occurrence gradient contribution to row  $i$  from the  $k$ -th occurrence of token  $i$ . In the coherent-signal limit, assume  $h_{i,k} = \mu_i$  for all occurrences  $k$ , where  $\mu_i$  is the constant per-occurrence gradient signal. With mean reduction over the batch, the row gradient is the random variable

$$g_i = \frac{1}{B} \sum_{k=1}^{K_i} h_{i,k} = \frac{K_i}{B} \mu_i, \quad \mathbb{E}[g_i] = p_i \mu_i,$$

so the mean update already scales linearly with token frequency. The empirical Fisher block for row  $i$  is the second moment of this row gradient, taken over the random batch composition,

$$F_i = \mathbb{E}[g_i g_i^\top] = \frac{\mathbb{E}[K_i^2]}{B^2} \mu_i \mu_i^\top = \left( p_i^2 + \frac{p_i(1-p_i)}{B} \right) \mu_i \mu_i^\top.$$

For  $Bp_i \gg 1$  the variance term is subleading, so up to the conditional row-direction curvature  $\mu_i \mu_i^\top$ ,

$$F_i \propto p_i^2.$$

Consequently, along the row's signal direction,

$$F_i^{-1} \propto \frac{1}{p_i^2}.$$

Therefore the full natural-gradient update scales as

$$F_i^{-1} g_i \propto \frac{1}{p_i^2} (p_i \mu_i) = \frac{1}{p_i} \mu_i.$$

By contrast, a square-root Fisher or RMS-style preconditioner uses

$$F_i^{-1/2} \propto \frac{1}{p_i},$$

and therefore

$$F_i^{-1/2} g_i \propto \frac{1}{p_i} (p_i \mu_i) = \mu_i.$$

Hence the square-root Fisher correction cancels the explicit token-frequency factor and produces a probability-isotropic row update, while the full inverse Fisher produces an additional rare-token amplification proportional to  $1/p_i$ . Equivalently, under this coherent full-batch frequency model,

$$g_i \propto p_i, \quad F_i \propto p_i^2, \quad F_i^{-1/2} g_i \propto p_i^0, \quad F_i^{-1} g_i \propto \frac{1}{p_i}.$$

## 6.9 Muon is the inverse square-root Fisher in the spectral basis

We can view Muon as applying the same square-root Fisher principle as Adam, but in the spectral basis of a matrix gradient rather than in the coordinate basis.

Consider a linear layer

$$y = Wx, \quad W \in \mathbb{R}^{m \times n},$$

with upstream gradient  $\delta \in \mathbb{R}^m$ . For a single example, the gradient with respect to  $W$  is the rank-1 outer product

$$G = \nabla_W \ell = \delta x^\top.$$

Vectorizing the matrix, the corresponding empirical Fisher contribution is

$$\text{vec}(G) \text{vec}(G)^\top.$$

Thus the full Fisher block for the layer is

$$F_W = \mathbb{E} [\text{vec}(G) \text{vec}(G)^\top].$$

This is the exact second-moment geometry of the layer gradient. Standard Adam keeps only its diagonal in the coordinate basis, using

$$\mathbb{E}[G_{ij}^2]$$

as the per-parameter curvature estimate and dividing each coordinate by the square root of this quantity.

Muon instead uses a matrix-valued second moment induced directly by the gradient matrix. Given a layer gradient  $G \in \mathbb{R}^{m \times n}$  with singular value decomposition

$$G = U \Sigma V^\top,$$

the right Gram matrix is

$$G^\top G = V \Sigma^2 V^\top.$$

This is the spectral analogue of the squared gradient  $g^2$ : its eigenvectors are the right singular directions of  $G$ , and its eigenvalues are the squared singular values. Therefore, applying the inverse square root gives

$$(G^\top G)^{-1/2} = V\Sigma^{-1}V^\top$$

on the nonzero spectrum. Right-conditioning the gradient by this matrix yields

$$G(G^\top G)^{-1/2} = U\Sigma V^\top (V\Sigma^2 V^\top)^{-1/2} = U\Sigma V^\top V\Sigma^{-1}V^\top = UV^\top.$$

This is exactly the polar factor used by Muon: all nonzero singular values of the gradient are normalized to one.

Thus Muon can be interpreted as square-root Fisher conditioning in the spectral basis. Adam divides each coordinate by the square root of its coordinate-wise gradient second moment,

$$g_i \mapsto \frac{g_i}{\sqrt{g_i^2}},$$

whereas Muon divides each singular direction by the square root of its spectral second moment,

$$G \mapsto G(G^\top G)^{-1/2}.$$

Equivalently, Adam normalizes gradient energy per coordinate, while Muon normalizes gradient energy per singular direction. This is why Muon produces the polar update  $UV^\top$ : it is the matrix-gradient analogue of casting the gradient into a square-root-Fisher-normalized, unitless update.

## 6.10 The LM-head factorizes like the embedding table

Per position, both gradients are rank-1 outer products (App. 6.6):

$$\nabla_E = e_i u^\top \quad (e_i \text{ one-hot}), \quad \nabla_{W^{\text{out}}} = \delta h^\top \quad (\delta_i = p_i - \mathbf{1}[y = i]).$$

Same structure gives the same factorization  $\mathbb{E}[g_{ij}^2] = R_i C_j$ , so Ember treats both identically. The only difference is row support: the embedding fires one row ( $e_i$  one-hot), while the head touches every row with weight  $p_i$  (the softmax mass). The head is thus a *smoothed* embedding—hard participation  $\mathbf{1}[\text{tok} = i]$  replaced by soft  $p_i$ —and  $\hat{r}_i$  estimates token participation in both (a count for the input table, an expected probability for the head). Early weight tying empirically confirms the correspondence.